THE JOURNAL OF PHYSICAL CHEMISTRY B

Article

pubs.acs.org/JPCB

Phase Diagram and Structures in Mixtures of Poly(styrenesulfonate anion) and Alkyltrimethylammonium Cations in Water: Significance of Specific Hydrophobic Interaction

Simona Sitar,[†] Bart Goderis,[‡] Per Hansson,[§] and Ksenija Kogej*[,†]

[†]Department of Chemistry and Biochemistry, Faculty of Chemistry and Chemical Technology, University of Ljubljana, Aškerčeva 5, PO Box 537, SI-1000 Ljubljana, Slovenia

[‡]Molecular and Nanomaterials, Department of Chemistry, Catholic University of Leuven, Celestijnenlaan 200F, B-3001 Heverlee, Belgium

[§]Department of Pharmacy, Biomedical Centre, Uppsala University, Box 580, SE-75123 Uppsala, Sweden

Supporting Information

ABSTRACT: Mixtures of polyelectrolytes and oppositely charged surfactants show very rich phase behavior that is influenced by surfactant−ion and polyion properties and by water content. A general feature is associative phase separation as a result of strong electrostatic interactions, whereas the effect of eventual more specific interactions (e.g., hydrophobic) has not been thoroughly investigated. In this paper, we report a detailed study on phase behavior and structures in poly(styrenesulfonate anion) (PSS^-)−cetyltrimethylammonium cation (CTA^+)−water mixtures that are characterized by a hydrophobic interaction between the styrene groups of PSS^- and the micelle interior. Structures of various phases were determined by small-angle X-ray scattering, and results indicated the presence of a disordered micellar and an ordered hexagonal phase; no cubic phase was found. The general conclusion is that the highlighted hydrophobic interaction promotes dissolution of CTAPSS when the polyion salt is added and provides further stabilization of the dense phase when the surfactant salt is added.

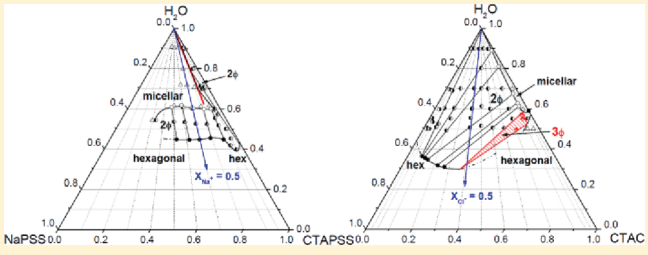

INTRODUCTION

In many applications, polyelectrolyte−surfactant mixtures are diluted by water from some concentrated formulation in order to deposit polyion−surfactant ion complexes (PSCs) as a protective layer on a surface. The complex phase separates out from the mixture upon dilution with water because the concentration of electrolyte screening the attraction between the polyion and the surfactant micelles decreases. In the simplest case, the screening electrolyte consists of the counterions to the polyion and the surfactant ion in the mixture. The stability and the structure/performance relationship of deposited layers formed in this way are expected to depend largely on the composition of the complexes. In this respect, the results from systematic phase studies have given important clues as to the importance of the overall composition of the phase separating mixture as well as to the properties of the components, such as surfactant counterion and tail length, and polyion molecular weight and charge density.[1−11] A less studied aspect is the influence of hydrophobic interactions between the polyion and surfactant micelles, although it has been investigated in some detail in cross-linked polyelectrolyte gel systems.[12−15] This type of interaction appears to promote the formation of soluble PSCs, another important field of application of polyelectrolyte−surfactant mixtures. Soluble complexes exist when the concentration of either polyelectrolyte or surfactant is in sufficient excess. It was recognized early that the presence of hydrophobic moieties on the polyion, both pendant alkyl chains and groups integrated in the polymer backbone, increased the solubility range in the polyelectrolyte-rich regime.[16−21] In particular, cationic surfactants and poly(styrenesulfonate) (PSS) have been reported to form soluble complexes in a wide range of compositions as long as the polyion is in some charge excess.[18,19,21] In the present work, a detailed phase study of the latter system is presented.

The most intelligible presentation of various events that may occur upon changing composition in a certain polyelectrolyte−surfactant−water system is in the form of a phase diagram. However, the construction of a phase diagram is a formidable task in such complex systems since a mixture of a polyelectrolyte (polyion, P, + counterion, M) and an oppositely charged surfactant (surfactant ion, S, + counterion, X) in water is a four-component system; the ionic species can be combined into four different electrolytes, which are reduced to three independent components by the electroneutrality condition. Thalberg et al.[22,23] pointed out that pseudo-three-component representations (MP + SX + water) in the form of conventional triangular phase diagrams can be misleading, and used a diagram in the shape of a tetragonal pyramid for a complete presentation of such systems, with the

Received: December 20, 2011
Revised: March 20, 2012
Published: March 21, 2012

   dx.doi.org/10.1021/jp212263b | J. Phys. Chem. B 2012, 116, 4634−4645

pure electroneutral species positioned at each apex. Later, Piculell et al.[5−10] demonstrated that essential information about the aqueous phase behavior can be obtained by mixing instead the surfactant ion−polyion complex salt (SP) with either MP or SX. The resulting phase behavior can be presented in two conventional triangular diagrams. These are referred to as the polyion-mixing plane (abbreviated herein as P-plane) and the surfactant ion-mixing plane (abbreviated as S-plane), respectively, since each make up one side of the four-component phase pyramid. In particular, these phase diagrams highlight how stable the surfactant ion−polyion complexes are in the presence of excess of polyelectrolyte or surfactant. Of course, they give no information about the screening effect of simple salt, which is important in applications, but clearly display the differences between polymeric and simple ions as counterions to the surfactant aggregates, with respect to phase stability. The same approach will also be undertaken here to investigate phase behavior in PSS−cationic surfactant−water mixtures.

PSS is a strong polyelectrolyte with benzene rings carrying the charged sulfonate groups. The aromatic rings assign the poly(styrenesulfonate anion) (PSS^-) a hydrophobic character. It has been shown by NMR measurements[24] that, in complexes with surfactants, the styrene group tends to incorporate into the hydrophobic interior of surfactant aggregates, thus making the polyion−surfactant interaction in the PSCs extremely strong and resistant to external conditions such as changing the ionic strength,[19] or to dynamic processes such as exposing the soluble (nonstoichiometric) PSC to direct current measurements.[18,21,25]

On first thought, the combination of strong electrostatic attraction and the highlighted and well documented[17,18,25−28] hydrophobic attraction between the surfactant and the polyion should strongly promote phase separation of the PSC already at low surfactant additions to the polyion (i.e., at low surfactant-to-polyion mixing ratios). However, studies in dilute solutions show[17,19,26] that PSS−surfactant systems remain homogeneous one-phase solutions even when up to 70% of the charged sulfonate groups have been neutralized by surfactant ions. Moreover, the width of this one-phase/homogeneous region seems to be independent of the simple salt concentration in a broad range of salt (NaCl) concentrations.[19] Another important feature is that a very large excess of surfactant is needed to dissolve the PSC[19] once precipitated. This is just the opposite to the situation with excess of the polyelectrolyte, where dissolution is easily achieved. Similar results can be deduced from an approximate pseudo phase diagram determined in PSS^- mixtures with dodecyltrimethylammonium bromide (DTAB) in water.[20] In that work, the conventional way of mixing PSS^- and DTA^+ salts was used, which produces different amounts of simple salt in solution, depending on the mixing ratio. Even though the phase diagram was far from being complete, it pointed to a very good solution stability of the PSS^-−DTA^+ aggregates, in agreement with the above findings. The conventional approach for the preparation of PSS−surfactant aggregates was employed also in structural studies,[29,30] which have identified two types of ordering of surfactant in these complexes, either in a disordered micellar form or in a highly ordered liquid crystalline-like hexagonal structure. These studies were conducted at high water contents, mostly in the polyelectrolyte-rich regime, and offered no insight into the solubilization mechanism.

Our objective therefore is to determine a complete phase diagram and structures of phases in a PSS−cationic surfactant−water system. The ultimate goal is to clarify the role that specific hydrophobic interaction between surfactant aggregates and the PSS^- anion play in structure formation and in overall phase behavior. To be able to detect effects related to the curvature of the micelles, we will compare the behavior of two surfactant analogues, dodecyltrimethylammonium chloride (DTAC) and cetyltrimethylammonium chloride (CTAC).

EXPERIMENTAL SECTION

Materials. Sodium poly(styrenesulfonate) (NaPSS; molar mass of the monomer unit M = 206 g/mol), with a nominal molecular weight of 70.000 g/mol (corresponding to around 340 monomer units) and a degree of sulfonation of 1.0, supplied by Polysciences Inc. Warrington, PA, was used as the starting material. NaPSS was first converted to poly(styrenesulfonic acid) (HPSS) by dialysis against HCl and then purified by dialysis against Millipore water followed by ultrafiltration. Finally, HPSS was concentrated by vacuum distillation. The concentration of the HPSS stock solution was determined by neutralization potentiometric titration. The purified HPSS was analyzed by dynamic light scattering in 0.2 M NaCl at 25 °C, which revealed a narrow size distribution with an average hydrodynamic radius of particles being around 4 nm.

CTAC (M = 320 g/mol) and DTAC (M = 264 g/mol) were purchased from Fluka Analytical and Fluka Chemica, respectively, and were used without further purification.

Preparation of Complex Salts. The complex salts of the PSS^- anion with the DTA^+ and CTA^+ cations, designated as DTAPSS and CTAPSS, respectively, were prepared according to the previously proposed procedures[5] by titrating the hydroxide form of the surfactants with HPSS. The first step was to convert C_nTAC (n = 12 and 16 for DTAC and CTAC, respectively) to C_nTAOH by ion exchange. The ion-exchange resin, Dowex MTO SRB LCM G Supelco, was charged by stirring it in excess amount of 1 M NaOH for 2 h and then rinsed with distilled water until the rinsing water reached pH ≈ 7. C_nTAC (7 g) was dissolved in a plastic beaker containing a large excess (150 mg) of resin and 100 mL of distilled water. The solution was stirred for 2 h, filtered, and the filtrate was rinsed with distilled water into a new batch of 150 mg of resin and 100 mL of water. This mixture was then stirred for another 2 h. The last step was repeated once more with a third fresh batch of resin. The final product was an alkaline solution of C_nTAOH. The absence of Cl^- ions in this solution was proven by the reaction with $AgNO_3$.

The freshly prepared solution of C_nTAOH was titrated drop by drop into the HPSS stock solution under stirring. The titration was continued until the equivalence point was reached, upon which a white precipitate was formed in solution. The equivalence point was determined from separate pH titration curves. The pH value at the equivalence point was 7.15 and 7.05 for DTAOH and CTAOH, respectively.

After equilibrating overnight, the solution with the precipitate was freeze-dried. The complex salt was obtained as a white and very light powder, which was put to storage over silica gel in a desiccator. Elemental analysis confirmed a 1:1 molar ratio between CTA^+ and SO_3^- groups in the complex.

Sample Preparation. *Mixtures of Complex Salt and Water.* Samples of DTAPSS or CTAPSS complex salt and water with water content between 25 and 98 wt % were prepared by weighing calculated amounts of substances into glass tubes. Samples were mixed for a short time with the Vortex vibrator and then centrifuged for 15 min in the centrifuge at 4000 rpm. Afterward, the tubes were flame-sealed and left to stand at 40 °C overnight. The next day, mixing in the centrifuge was continued for 5 h with turning the tubes end over end every 30 min.

dx.doi.org/10.1021/jp212263b | J. Phys. Chem. B 2012, 116, 4634−4645

The samples were then kept in an oven at 40 °C in order to decrease their viscosity to facilitate mixing of components. Since the systems, particularly at low water content, are very viscous, the heating cycles represent an important stage in the sample preparation process. For samples with high water content (low viscosity), one day at elevated temperature was normally sufficient, whereas for those with low water content (high viscosity) the heating time was prolonged up to 10 days, if required. After heating, centrifugation was repeated, but this time the tubes were no longer turned end over end. Samples prepared in this way were left to equilibrate at 25 °C between 3 and 6 months, depending on sample viscosity and appearance. The described handling procedure is very important, because thoroughly mixed components are essential for the proper separation of phases.

Mixtures of Complex Salt, Polyelectrolyte (or Surfactant), and Water. In addition to complex salt−water mixtures, samples of the complex salt, water, and polyelectrolyte (NaPSS) or surfactant (CTAC) were prepared as well. In this part, only the complex salt with the longer chain surfactant, CTAPSS (molar mass per monomer unit M = 467 g/mol), was used. Again, appropriate amounts of the complex salt, the polyelectrolyte, or the surfactant and water were weighted into glass tubes. The mixing procedure was the same as that described above. Samples with water content higher than 70 wt % were easy to handle, whereas those with lower water content required longer equilibration times and more careful treatment. In addition, high viscosity was more problematic for mixtures with excess of the polyelectrolyte, while excess of the surfactant resulted in a decreased viscosity and easier manipulation of samples.

Determination of Compositions and Structures of Phases. The characterization of samples was first carried out by visual inspection in normal light and through crossed polarizers to detect optically anisotropic phase (in the present case the hexagonal phase). Further, structures were characterized by small-angle X-ray scattering (SAXS). SAXS measurements were conducted using two SAXS setups: the synchrotron SAXS at the Dutch-Belgian Beamline BM26B of the European Synchrotron Radiation Facility (ESRF) in Grenoble, and a high performance SAXS instrument "SAXSess" from Anton Paar KG, Graz, Austria. The block-collimating unit of the latter system was attached to a conventional X-ray generator (Philips, Holland) equipped with a sealed X-ray tube (Cu anode target type producing Cu Kα X-rays with a wavelength of 0.154 nm) operating at 35 kV and 35 mA. The scattered X-ray intensities were measured with a linear position sensitive detector. Liquid-like samples were filled in capillaries, whereas for dense phases, special sample holders for pastes and powders SWAXS from Hecus were used. The synchrotron experiments were executed at a wavelength of λ = 0.775 Å. A two-dimensional (2D) multiwire gas-filled detector was placed at 1.5 m from the sample after an evacuated tube. The reflections of a silver behenate standard were used to calibrate the scattering angles,[31] expressed as a function of the scattering vector q, with $q = 4\pi \sin\theta/\lambda$ and θ being half of the scattering angle. Data were accumulated at room temperature for 60 s with the samples being presented in a rubber ring, sandwiched between thin mica sheets. The sandwich construction was kept together in an aluminum frame, which ensures a sample thickness of 1 mm. The SAXS patterns were normalized to the intensity of the incoming beam, measured by an ionization chamber placed downstream from the sample, and corrected for the detector response prior to azimuthally averaging the isotropic data using the homemade software ConeX.[32] Finally, the patterns were corrected for the scattering due to the empty setup, taking into account the sample and sample holder transmission.

The phase-separated samples from the two-phase regions were analyzed for compositions. The analysis was performed for the dilute phase, except when its amount was not sufficient. In this case, the dense phase was analyzed. For the determination of water content the Karl Fischer method was used. The concentration of PSS^- anion was determined spectrophotometrically by measuring the absorbance of UV light with a wavelength of 261.5 nm, and the concentration of Cl^- ions was assessed by potentiometric titration using $AgNO_3$ as a titrant. From known structures and compositions, the phase diagram was constructed in the polyion and in the surfactant ion mixing planes. For biphasic samples that did not phase-separate macroscopically (systems with low amount of water, similar density of phases), the composition determination was not possible. In these cases, phase boundaries were mapped by following the SAXS structural data. All compositions are given in weight % (wt%).

RESULTS

Binary Mixtures of Stoichiometric Complexes and Water. To better understand the structures that are formed when the CTA^+ (DTA^+) micelles bind to PSS^- anions, we first studied structures in mixtures of CTAPSS (or DTAPSS) and H_2O. The solubility of CTAPSS in water is very low, as ascertained by the spectroscopic analysis of PSS^- concentration in water saturated with the complex and also by the scattering intensity of the equilibrium water solution, which was on the level of pure water. The solubility of DTAPSS is higher, as indicated by a well pronounced micellar peak in the SAXS curve of the DTAPSS saturated water.

The sequence of structures in mixtures of DTAPSS and CTAPSS and water is shown in Figure 1. Only the disordered

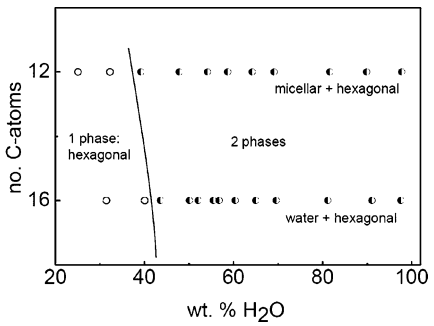

Figure 1. Sequence of phases for binary mixtures of complex salts, DTAPSS and CTAPSS, and water. The y-axis gives the number of C-atoms in surfactant's alkyl chain (n = 12 and 16 in DTAPSS and CTAPSS, respectively).

micellar (DTAPSS) or almost pure water (CTAPSS) and the ordered hexagonal phase were detected. The transition from the one-phase region of the hexagonal phase to the two-phase region of coexisting hexagonal and micellar (or water) phases was found at around 40 (DTAPSS) or 43 wt % of water (CTAPSS). In units of micelle (nonpolar) volume fraction, these concentrations are nearly identical. This insensitivity of the boundary delimiting the one phase hexagonal region (at low water contents) from the two-phase hexagonal−micellar coexistence (at higher water contents) to surfactant chain length is in line with observations reported in the literature for

dx.doi.org/10.1021/jp212263b | J. Phys. Chem. B 2012, 116, 4634−4645

C_nTA^+ complexes with the polyacrylate anion (PA^-) having long polymer chains (6000 repeating units).[7] Here also, the phase boundary between one-phase hexagonal and either the two-phase hexagonal/micellar (CTAPA) or one-phase cubic region (DTAPA) was found at around 42 (DTAPA) to 43 wt % H_2O (CTAPA). However, the difference is in the appearance of the cubic phase in the DTAPA case, which was not detected in the DTAPSS case. This difference is attributed to specific hydrophobic interaction between PSS and surfactant micelles, i.e., to incorporation of styrene groups into micellar surface. In combination with electrostatic interaction, this provides a strongly reinforced attraction that produces concentrations where hexagonal structure is the preferred packing of surfactant into aggregates. PSS also affects the curvature of micelles by its involvement in micelle formation (as will be further discussed below). Note that the hexagonal structure normally appears at high surfactant concentrations in solution (above 50 wt %). Because hexagonal patterns of DTAPSS were less explicit than those of CTAPSS, the overall phase behavior was subsequently studied for CTAPSS complexes.

The samples of the complex salt CTAPSS containing less than 43 wt % of H_2O are one-phase and form a hexagonal (H_1) structure. The SAXS pattern of the one-phase hexagonal CTAPSS sample with 31 wt % of H_2O is shown in Figure 2a

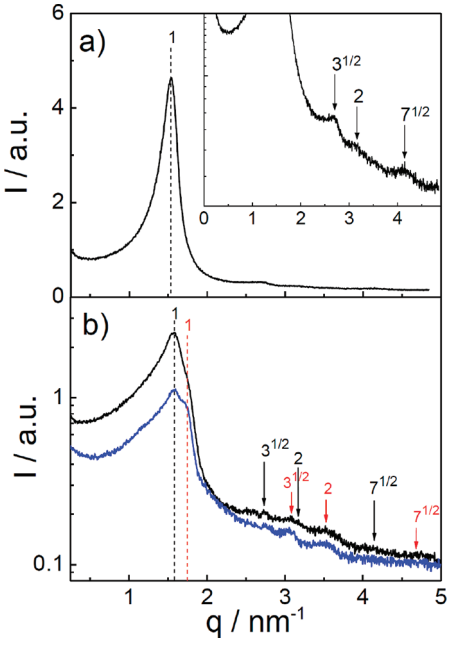

Figure 2. SAXS patterns of the hexagonal phase in (a) a one-phase hexagonal CTAPSS sample with 31 wt % of water and in (b) two two-phase CTAPSS samples containing 50 (black curve) and 60 (blue curve) wt% of water. Arrows indicate peak positions.

and clearly displays a strong first-order hexagonal peak at $q \approx 1.54$ nm^{-1} and additional higher order peaks that fit the characteristic sequence $1:\sqrt{3}:\sqrt{4}:\sqrt{7}$ for the hexagonal H_1 phase (see the inset in Figure 2a).

An increase in water content in binary CTAPSS–H_2O mixtures above 43 wt % induces a separation into two phases: the upper, virtually pure water, phase and the bottom hexagonal phase of a powder-like appearance. The lower the water content, the more difficult the separation of phases. Thus, two macroscopically separated phases are seen for water contents above 70 wt %, whereas for lower water contents, the water phase remains trapped in the hexagonal phase and gives it a whitish appearance.

The dense phases of all CTAPSS–H_2O samples from the two-phase region displayed hexagonal patterns resembling the ones in Figure 2b. SAXS patterns clearly display the main peak at $q \approx 1.57$ nm^{-1} (indicated by a black dashed line), which is accompanied by three higher order peaks (indicated by black arrows), whereas the other indicated peaks (see red arrows) actually fit the sequence to a main peak at a somewhat higher q, i.e., at $q \approx 1.77$ nm^{-1}, a peak that is superimposed on the main peak (see the red dashed line that indicates an approximate position of this peak). This might be an indication of another hexagonal structure in these samples. However, according to the phase rule, there can be no more than two phases in a two-component system (the complex salt and water) at constant temperature and pressure. Possible interpretations are that samples either contain more than two components (e.g., due to polyion polydispersity) or that they are not completely equilibrated. We emphasize that the same complex scattering patterns were observed also for dense phases of the binary CTAPSS–H_2O mixtures with higher water content, where mixing of the components was not problematic, and even after repeated sample preparation with a new batch of the complex salt by extending the time of sample equilibration. On the contrary, samples that did not contain a macroscopically separated dilute phase displayed clear hexagonal patterns (c.f. Figure 2a). We will come back to this point when discussing similar scattering patters for ternary samples on the S-plane with a small amount of added excess CTAC.

The Polyion-Mixing Plane. The triangular phase diagram in the P-plane is shown in Figure 3a. Most of biphasic samples on this plane separated easily into two phases, except samples from the region with density inversion (see below). The diagram is based on approximately 60 samples and contains a peculiarly shaped two-phase region extending out from the CTAPSS–H_2O axis. Above that region, there is a disordered micellar (L_1) one-phase region with water content above 60 wt %, and below is an ordered hexagonal (H_1) phase with water content below around 45 wt %. It is worthwhile to stress that no cubic phase was found at any composition. However, other types of phases, e.g., lamellar, are expected at water contents lower than those examined here.

The CTAPSS-rich part of the irregularly shaped two-phase region is a narrow area close to the CTAPSS-H_2O axis extending between cca 45 and 100 wt % of water. The feature of this area is the coexistence of an upper (L_1) phase, containing the dissolved nonstoichiometric complex, and a bottom (H_1) phase, which is close in composition to the stoichiometric complex (tie lines connecting the phase separated samples are tilted to the left). The border to the L_1 phase in the upper part of the diagram is positioned at a weight ratio CTAPSS:NaPSS around 8.4:1.6, which corresponds to a molar fraction of Na^+ ions in the counterion population of the nonstoichiometric (Na,CTA)PSS complex $X_{Na+} = 0.3$ (or less; c.f. the shrinking of this part of the two-phase region for water contents around 60 wt % to lower X_{Na+}). Evidently, the complex salt is easily dissolved by adding an excess of the polyelectrolyte. The same result on the solubility of the complex salt was obtained previously for complexes of PSS^- anion and cetylpyridinum cations (CP^+) in relatively dilute solutions.[21]

The NaPSS-rich part of the two-phase region is a broad region of coexistence of L_1 and H_1 at water contents between around 45 and 60 wt %, which extends, at least, to CTAPSS:NaPSS weight ratios around 3.5:6.9 or $X_{Na+} = 0.77$ (note that the sample with 55 wt % of H_2O and a mixing ratio CTAPSS:NaPSS = 3:7 is

dx.doi.org/10.1021/jp212263b | J. Phys. Chem. B 2012, 116, 4634–4645

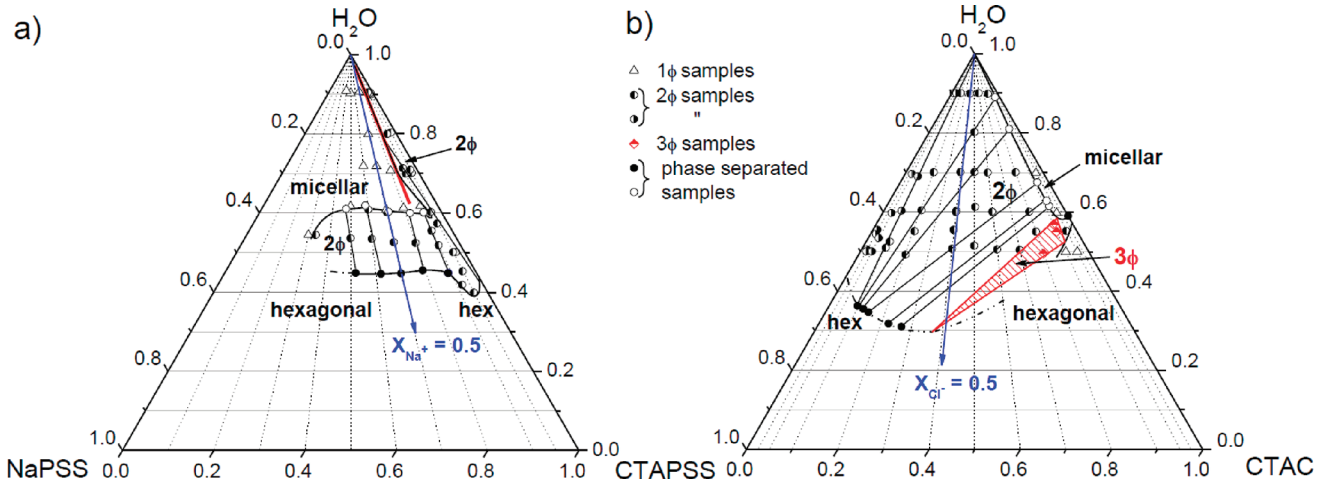

Figure 3. Ternary phase diagrams of NaPSS/CTAPSS/H_2O (a) and CTAPSS/CTAC/H_2O (b) mixtures at 25 °C. Compositions are given in wt %. The arrow on the P-plane (NaPSS/CTAPSS/H_2O mixtures) indicates the value $X_{Na+} = 0.5$ for the mole fraction of sodium ions in nonstoichiometric (Na,CTA)PSS complexes, whereas the one on the S-plane (CTAPSS/CTAC/H_2O mixtures) indicates the value $X_{Cl-} = 0.5$ for the mole fraction of chloride ions in CTA(Cl,PSS)−water mixtures. The red line on the P-plane indicates the value $X_{Na+} = 0.3$ or $f = 1.4$ (see text). Biphasic samples in different parts of the two-phase region on the S-plane are indicated by either ◑ or ◐ (see text).

monophasic with a disordered micellar structure, whereas samples with higher NaPSS content were not investigated). In this region, the separation of phases is of an associative type (both salt components are enriched in the dense phase) with almost the same composition of the nonstoichiometric (Na,CTA)PSS complex in the coexisting phases (X_{Na+} is approximately the same in L_1 and H_1). Interestingly, the transition from the CTAPSS-rich to the NaPSS-rich part is accompanied by a density inversion, viz., the water-poor H_1 becomes the top phase and L_1 is the bottom phase. Examples of hexagonal patterns of samples from this broad two-phase region are shown in Figure 4 with the first-order hexagonal peak found at

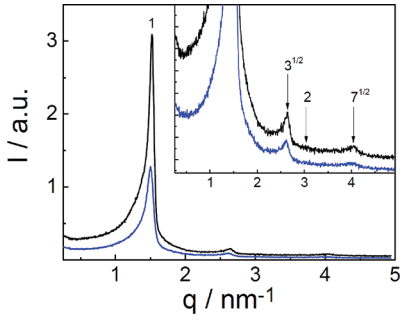

Figure 4. SAXS patterns of the hexagonal phase for two samples with an overall amount of water around 50 wt % and the CTAPSS:NaPSS weight ratios 7:3 (black curve) and 9:1 (blue curve). In the inset higher order peaks are indicated.

$q = 1.53$ nm^{-1}. The transition between the two parts takes place in the range of CTAPSS:NaPSS weight ratios between 9:1 and 19:1 and at water contents of 40−60 wt %. Macroscopic phase-separation in samples corresponding to these compositions was impossible to achieve even after prolonged equilibration and repeated centrifugation of samples at 4000 rpm, presumably due to very similar density values of the coexisting phases. We have concluded that this is the region where density inversion takes place. Another possibility for the transition between the narrow and the broad two-phase region would be an interconnecting three-phase region of coexistence of one L_1 and two hexagonal phases. However, SAXS patterns of these samples did not confirm this possibility.

Representative SAXS curves of samples containing 40−50 wt % of water and having CTAPSS:NaPSS weight ratios 19:1 and 9:1 are shown in Figure 5. They mostly display a broad micellar

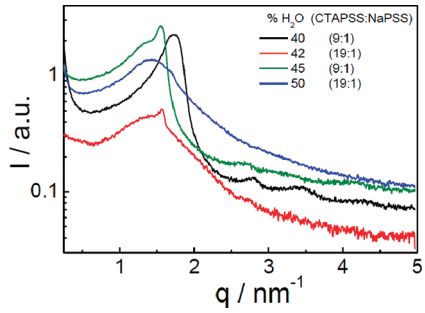

Figure 5. SAXS patterns of samples with water content between 40 and 50 wt % and CTAPSS:NaPSS weight ratios 19:1 or 9:1.

peak and a superimposed hexagonal peak, which is most clear in the 40 wt % sample that is the closest to the border with the hexagonal phase. The proportions of both patterns depended on the overall composition of samples and also on the sampling procedure.

The Surfactant−Ion Mixing Plane. The triangular phase diagram in the S-plane is shown in Figure 3b. It is based on around 100 samples. The most striking observation is that, for water contents above 60 wt %, the homogeneous liquid phase (L_1) exists only at weight ratios of CTAPSS to CTAC below around 1:9. This means that a large excess of CTAC has to be added to solubilize/dissolve the complex salt: around 13 or even up to almost 30 mols of CTAC per 1 mol of CTAPSS at low (70 wt %) or at high (90 wt %) water content, respectively. On the P-plane, only 0.4 mols (or down to 0.11 mols) of NaPSS were sufficient to dissolve 1 mol of CTAPSS in solutions with more than 60 wt % of water.

There are two one-phase regions, a very broad two-phase region, and a clear three-phase region on this plane. The one-phase regions are the hexagonal (H_1) phase, occupying the

dx.doi.org/10.1021/jp212263b | J. Phys. Chem. B 2012, 116, 4634−4645

entire lower part of the plane (at water contents below 50–30 wt %, depending on the CTAPSS:CTAC mixing ratio), and the micellar (L_1) phase that is limited to a narrow area close to the CTAC-H_2O axis at water contents above 59 wt %. The boundary between the two-phase region of L_1–H_1 coexistence and the homogeneous L_1-phase was obtained in two ways: (i) from the determined compositions of L_1-phases and (ii) by gradually adding CTAPSS to 20 and 30 wt % CTAC solutions (of relatively low viscosity in order to facilitate mixing), thus changing the composition along the line pointing to the CTAPSS corner. After each CTAPSS addition, the samples were thoroughly mixed, left to equilibrate, and examined in order to detect the appearance of a new phase. The point where traces of a new phase were detected (this may be taken as the phase boundary with the two-phase region) agreed with the phase boundary position obtained from the determined sample compositions.

The transition from L_1 to H_1 in pure CTAC solutions was found at around 41–42 wt % of CTAC (or 58–59 wt % H_2O), in agreement with reports in the literature.[33] A clear three-phase region appears on the surfactant-rich side at water contents below cca 60 wt %.

The Narrow Part of the Hexagonal/Micellar Region along the CTAPSS-H_2O Axis. The part of the diagram with CTAPSS:CTAC ≥ 9:1, adjoining the CTAPSS-H_2O axis, displays distinctive differences in comparison with the rest of the S-plane and is therefore discussed separately. In this part, there is a coexistence of a dilute upper phase (virtually pure water or a very dilute CTAC solution) and a dense bottom phase. For water contents below 70 wt %, macroscopic phase separation was not achieved; the dilute phase remained trapped in the dense phase.

SAXS patterns of samples with 50 wt % of H_2O from this region are shown in Figure 6 for three mixing ratios between CTAPSS and CTAC (i.e., CTAPSS:CTAC between 39:1 and 9:1). They resemble the previously reported hexagonal patterns for the binary CTAPSS-H_2O mixtures (c.f. Figure 2b). Two hexagonal patterns, both exhibiting at least five peaks (see the black and red arrows indicating peak positions), were detected with the main hexagonal peaks found at closely positioned q values, i.e., at q = 1.57 and 1.74 nm^{-1}. The new emerging peak at q = 1.74 nm^{-1} corresponds to a smaller characteristic distance d (= 3.7 nm) in comparison with the peak at q = 1.57 nm^{-1} (d = 4.0 nm), suggesting that doping of CTAPSS with small amounts of CTAC decreases the distance between surfactant cylinders.

Some samples with the mixing ratio CTAPSS:CTAC = 9:1 still display both peaks, but others display only the peak at an intermediate q (= 1.65 - 1.67 nm^{-1}; compare curves in Figure 6a,b for CTAPSS:CTAC = 9:1). The relative height of the peak at q = 1.74 nm^{-1} increases with increasing CTAC content. It should be emphasized that similar complex SAXS patterns, indicating two hexagonal structures, were obtained also for the dense phases of samples containing the same proportions of complex salt and surfactant (CTAPSS:CTAC ≥ 9:1) but having a higher water content (70–90 wt % H_2O), in which the dilute and the dense phase separated easily and where presumably the attainment of phase equilibrium was not problematic. The samples indicating two hexagonal structures in the dense phase are designated in Figure 3b by (right-)half-filled circles (◑).

The simplest interpretation of the above observations would be that samples with CTACPSS:CTAC ≥ 9:1 are triphasic. It is, however, difficult to see the motivation of the system to form two hexagonal phases with very close q (or d) values in equilibrium. However, also hexagonal patterns of samples from the biphasic region, with more CTAC added, displayed two overlapping patterns in the dense phase (but with different second q value; see below), which suggests that this may be a feature requiring a unified interpretation that will be given in the Discussion section.

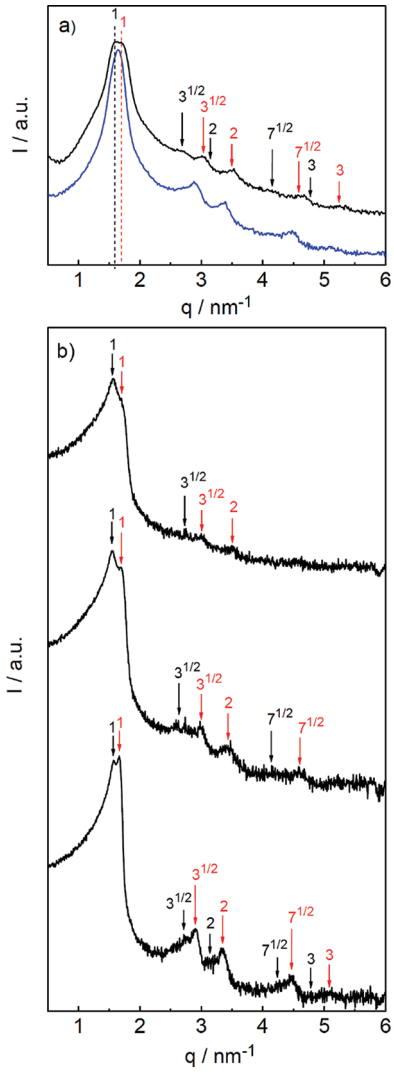

Figure 6. (a) SAXS patterns of the dense hexagonal phase for two samples with 50 wt % of water and CTAPSS:CTAC weight ratio 39:1 (black curve) and 9:1 (blue curve): these patterns were taken on the synchrotron. (b) SAXS patterns of a new batch of samples with 50 wt % of water, taken on the Kratky system. CTAPSS:CTAC ratios from top to bottom: CTAPSS:CTAC = 39:1, 19:1 and 9:1.

The Broad Part of the Hexagonal/Micellar Two-Phase Region. To the right of CTAPSS:CTAC = 9:1 extends a very broad L_1–H_1 two-phase region that occupies the majority of the upper part of the surfactant plane. In this region, phase separation is mainly of a segregative type: samples separate into dense CTAPSS-rich and dilute CTAC-rich phase (see the tie lines for some samples in this region that are evidently tilted to the right). The motivation to describe this type of phase separation as segregation is its resemblance with segregating polymer mixtures. Namely, CTAPSS-CTAC mixtures separate into a phase rich in CTAPSS complex salt (which can be treated as component 1) and a phase rich in CTAC micelles (which can be treated as component 2). Although the

dx.doi.org/10.1021/jp212263b | J. Phys. Chem. B 2012, 116, 4634–4645

interaction between PSS^- and CTA^+ is strongly associative, CTAC and CTAPSS clearly tend to segregate in water. The complex salt is reluctant to incorporate CTAC into its structure and thus, in excess of water, CTAC accumulates in the dilute phase with a composition close to the CTAC–H_2O axis. By doing this, it removes some water from the hexagonal phase, a feature that will be discussed later.

SAXS patterns of the ordered bottom phase again displayed two overlapping scattering patterns. Examples of SAXS curves of dense phases in samples with 90 and 70 wt % of H_2O (note that this water content is relatively high) and CTAPSS:CTAC weight ratios 8:2, 6:4 and 2:8 are shown in Figure 7. They show

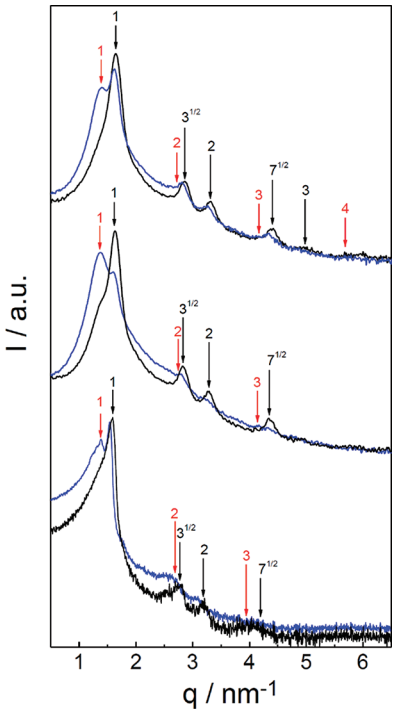

Figure 7. SAXS patterns of the bottom phase in samples containing 90 (black curves) and 70 wt % of water (blue curves); from top to bottom: CTAPSS:CTAC = 8:2, 6:4, and 2:8.

two overlapping strong first-order peaks, one at q = 1.65 nm^{-1} (indicated by a black arrow), and another one at q = 1.36 nm^{-1} (indicated by a red arrow), which was not seen in samples from the narrow region along the CTAPSS–H_2O axis. Well-defined higher order peaks (see black arrows) fit the characteristic sequence for a hexagonal pattern with the main peak at 1.65 nm^{-1}. Considerably more faint peaks can be traced as well, which, together with the main peak at 1.36 nm^{-1} (see red arrows), fit the characteristic scattering pattern of a lamellar phase.

Considering the low water content in dense phases (close to 30 wt %), the formation of a lamellar phase is not unrealistic. At 25 °C, H_1 in pure CTAC–H_2O solutions extends almost down to 30 wt % of water but is followed, at even lower water contents, by various other phases (gel phase, anisotropic intermediate phases).[33] The lamellar phase appears at higher temperatures (above cca 40 °C) and for water contents below approximately 20 wt %. However, in the presence of PSS^-, which is expected to occupy part of the volume between micelles, transition from H_1 to phases with lower curvature can be expected already at higher water contents. Note that we did not examine the part of the phase diagram with an overall water content below 30 wt % by direct preparation of such samples due to exceptionally difficult handling and equilibration in such systems. In general, when the complex phase or the sample as a whole contains very little water one can expect to find dense long-lived nonequilibrium structures. In this context, it is important that, although the additional peak at 1.36 nm^{-1} is identifiable both at high (90 wt %) and low (50 wt %) water content, it is more prominent at low water contents. Of course, as for the binary samples, a polydispersity of the polymer can always, in principle, give rise to multiphasic samples. Clearly, if the complexes actually contain H_1 in *equilibrium* with, e.g., a lamellar phase, this part of the phase diagram must contain a sequence of (narrow) three- and two-phase regions. Speaking against this is the progression of the position of the broad micellar peak (not shown) in the SAXS patterns from the L_1 samples. As the overall composition changed from the upper left side of the phase diagram toward the CTAC–H_2O axis, the characteristic q values of these peaks gradually increased (d values decreased) with a concomitant decrease in water content in L_1; the compositions of some of these L_1 phases are indicated by open circles in Figure 3b. They show that the phase equilibrium is characterized by one degree of freedom consistent with a two-phase region.

Although we are not in a position to completely settle these matters, we shall, for the remaining discussion, treat the whole broad part of the phase diagram on the S-plane, extending from the CTAPSS–H_2O axis to the L_1 monophasic region, as an H_1–L_1 biphasic region.

Three-Phase Hexagonal/Micellar/Hexagonal Region. A clear three-phase region was detected on the right side of the surfactant plane; it consists of two H_1 phases and an L_1 phase, which were perfectly separated. The two H_1 phases are the CTAPSS-rich phase (the bottom one with q = 1.62 nm^{-1} or d = 3.9 nm) and the surfactant-rich phase (the upper one with q = 1.44 nm^{-1} or d = 4.4 nm). The L_1 phase is the middle one with the broad micellar peak at q = 1.29 nm^{-1} (d = 4.8 nm). Scattering patterns of these phases are shown in Figure 8.

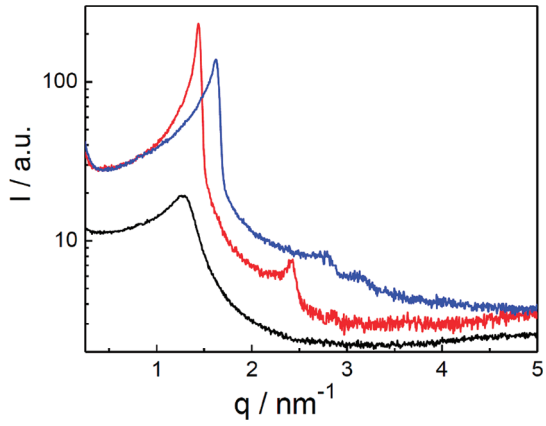

Figure 8. Scattering patterns of well-separated phases in a three-phase sample with 55 wt % of water and CTAPSS:CTAC weight ratio 1:9. Red curve shows scattering pattern of the upper (CTAC-rich) hexagonal phase, blue curve shows that of the bottom (CTAPSS-rich) hexagonal phase, and black curve shows that of the middle micellar phase.

The sample with 55 wt % of water and CTAPSS:CTAC = 1:19 contains two H_1 phases in equilibrium. Samples with 50 wt % of water and CTAPSS:CTAC ratio 1:9 and 1:19 are again homogeneous one-phase cases (see open triangles in Figure 3b) and have hexagonal structure, as shown in Figure 9 for the

dx.doi.org/10.1021/jp212263b | J. Phys. Chem. B 2012, 116, 4634–4645

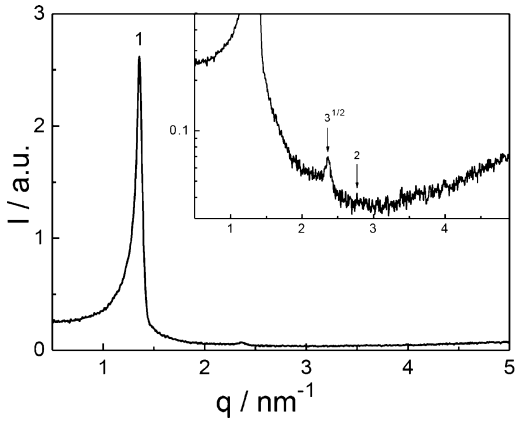

Figure 9. Scattering pattern of a one-phase sample with 50 wt % of water and a CTAPSS:CTAC weight ratio 1:9.

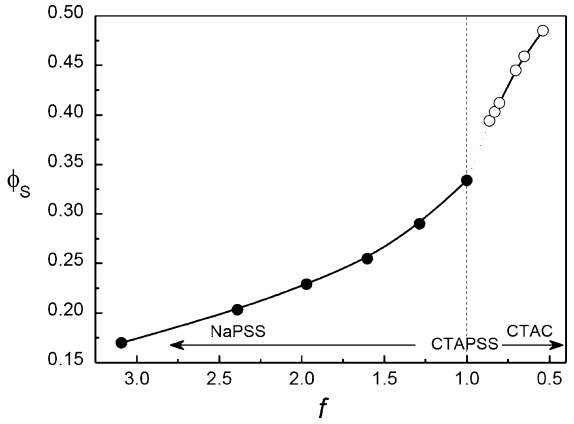

Figure 10. Apparent volume fraction, ϕ_S, of surfactant aggregates in hexagonal phases on the polyion ($f > 1$) and surfactant ion ($f < 1$) mixing plane. Note that the abscissa is plotted in the direction of decreasing f (this direction corresponds to triangular phase diagrams in Figure 3a,b), i.e., from NaPSS-rich to CTAC-rich samples.

CTAPSS:CTAC = 1:9 case, with the main peak at $q \approx 1.35$ nm^{-1} ($d \approx 4.65$ nm).

Relationship between Hexagonal Phases in Both Mixing Planes. In order to discuss the effect of adding CTAPSS to CTAC (NaPSS), or vice versa, we define the following parameters:

(i) Mole fraction of sodium ions, X_{Na+}, in the counterion population of the PSS$^-$ anion in complexes on the P-plane as $X_{Na^+} = n_{Na^+}/(n_{Na^+} + n_{CTA^+})$. Therefore, $X_{CTA^+}(= 1 - X_{Na^+})$ represents the fraction of charged groups on the polyion that are "neutralized" by surfactant micelles. The value $X_{Na^+} = 0.5$ is indicated in Figure 3a (see the blue arrow pointing from the water corner to the NaPSS/CTAPSS axis).

(ii) Mole fraction of monomeric Cl$^-$ ions, X_{Cl^-}, in the counterion population of the CTA$^+$ micelles as $X_{Cl^-} = n_{Cl^-}/(n_{Cl^-} + n_{SS^-})$; $X_{SS^-}(= 1 - X_{Cl^-})$ is the corresponding mole fraction of the polymeric counterions. The value $X_{Cl^-} = 0.5$ is indicated in Figure 3b (see the blue arrow pointing from the water corner to the CTAPSS/CTAC axis).

(iii) $f = n_{SS^-}/n_{CTA^+}$; $f = (X_{CTA^+})^{-1}$ in the P-plane and $f = X_{SS^-} = n_{SS^-}/(n_{SS^-} + n_{Cl^-})$ in the S-plane; f decreases from infinity to zero as the composition changes from pure NaPSS to pure CTAC, and is equal to 1 for pure CTAPSS.

Phase diagram in the P-plane (Figure 3a) can be redrawn by plotting X_{Na^+} as a function of the total weight fraction of solid (see Figure S1 in the Supporting Information). X_{Na^+} corresponds to the fraction of "free" polyion charges in complexes and is thus the relevant parameter in tuning the interactions on this plane. Figure S1 reveals that both a decrease in X_{Na^+} (or f) and an increase in the total amount of solid cause a transformation of the homogeneous micellar phase into a two-phase region. Additional discussion of the plot in Figure S1 can be found in the Supporting Information.

Figure 10 shows volume fraction of surfactant aggregates, ϕ_S, in hexagonal phases of phase-separated samples from the two-phase regions on both planes plotted as a function of f. The value of ϕ_S was estimated from the molar concentration of CTA$^+$ in the dense phases by assuming that the density of samples is 1 g/mL and that all surfactant is present in the aggregated form (the concentration of surfactant monomers was neglected). In this calculation, only the volume fraction of surfactant hydrocarbon tails (according to the Tanford relationship[34]) without the head groups was taken into account. Also, the contribution of embedded PSS anion to ϕ_S was ignored. Therefore, the calculated ϕ_S values should be considered as apparent. It can be seen from Figure 10 that ϕ_S in the dense phase increases with decreasing f, i.e., with increasing CTA$^+$ content over the whole range of f values.

Along with ϕ_S, the center-to-center distance, h, between cylinders and their apparent radius, r, were calculated from the position of the first diffraction peak, q_1:

$$h = \frac{2}{\sqrt{3}}\frac{2\pi}{q_1} \qquad r = \sqrt{\frac{2\phi_S}{\pi\sqrt{3}}}\frac{2\pi}{q_1}$$

A plot of h and r versus ϕ_S is shown in Figure 11. The radius r of cylinders increases with increasing volume fraction (i.e., with decreasing f) of CTAC aggregates in the hexagonal phase from around 1 nm to around 1.6 nm. For comparison, the radii of pure cylindrical CTA$^+$ micelles in water with two different counterions, chloride (Cl$^-$, $r = 1.62$ nm at $\phi_S \approx 0.36$; data for CTAC from this work) and acetate (Ac$^-$, $r = 1.78$ nm at $\phi_S \approx 0.49$;

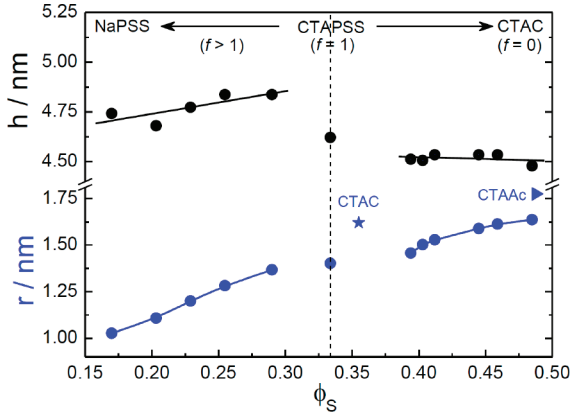

Figure 11. The center-to-center distance between cylinders, h, and the apparent cylinder radius, r, in hexagonal phases on the P- ($f > 1$) and on the S-plane ($f < 1$) as a function of the volume fraction of surfactant, ϕ_S. The blue star shows cylinder radius in a 42 wt % aqueous CTAC solution (this work), and the blue triangle shows its value in an aqueous CTAAc solution (taken from reference 4).

dx.doi.org/10.1021/jp212263b | J. Phys. Chem. B 2012, 116, 4634–4645

literature data for CTAAc[4]), are included in the figure. CTA^+ micelles in the presence of PSS^- are evidently smaller than the free ones. On the other hand, the distance h between the rods does not depend much on ϕ_S: it is around 4.75 nm (and slightly increases with ϕ_S) on the P-plane ($f > 1$) and drops to an almost constant value of 4.5 nm on the surfactant ion mixing plane ($f < 1$).

DISCUSSION

P-plane. One striking feature of the phase diagram in Figure 3a is the small amount of NaPSS required to completely dissolve CTAPSS in the L_1 phase. For water contents between 50 and 100 wt %, the phase boundary of the micellar (L_1) phase coincides with the line $f = 1.4$ (red line in Figure 3a), showing that the excess of PSS^- over CTA^+ needed for complex dissolution is remarkably constant. Another striking feature is the width of the biphasic region in the middle of the phase diagram, which is larger than expected for an L_1-H_1 transition driven by aggregate repulsion only. Both features can be related to the strong tendency of the PSS chains and the surfactant aggregates to associate with each other. As already noted, there is a hydrophobic motive for this due to the nonpolar character of the PSS side groups. This can explain the difference in behavior compared with polyelectrolytes with hydrophilic backbones, e.g., sodium polyacrylate (NaPA), interacting with the micelles mainly by electrostatic forces.

To make our point, we first note that the electrostatic interaction promotes not only the association between polyion and micelles but also the formation of dense phases ensuring good charge compensation of all ionic species. The stability of complex salts of PA and cationic surfactant ions in pure water[6,7] shows that the cohesive electrostatic force is strong enough to balance the swelling force due to the entropy of mixing also in very dense phases. This has been analyzed in detail elsewhere.[6,35] When polyelectrolyte is added, its incorporation into the complex phase should be favored by electrostatic energy but limited by entropy, promoting a uniform distribution of the small ions. The latter influence is consistent with the fairly uniform distribution of NaPA between the dilute and dense phases observed in the system of NaPA−CTAPA−H_2O. This leads to a scenario where, at low NaPA contents, CTAPA remains almost quantitatively in the dense phase but, at larger contents, the difference in composition between the coexisting phases decreases and finally vanishes in a critical point. Thus the dissolution of CTAPA by NaPA is accompanied by a gradual swelling of the dense phase. This is in sharp contrast to the behavior in Figure 3a, where, in the corresponding biphasic region, the dense phase does not swell, and the dissolution takes place at similar but more or less fixed polyion-to-surfactant ion charge ratios in both phases, thus $f \approx 1$ in the dense phase and $f \approx 1.4$ in the dilute phase. We believe that the tendency to conserve f, which also characterizes the L_1-H_1 transition at lower water contents, is imposed by the hydrophobic interaction. There is a strong tendency to maximize the contact between the PSS backbone and the hydrocarbon core of the micelles. There is plenty of evidence of the intimate contact between the PSS backbone and the hydrocarbon core of the micelles in dilute dispersions (see below). Clearly, the separation out of a phase with $f \approx 1$ from a dilute phase with $f \gg 1$, as in the PA case, would decrease the contact between PSS chains and micelles. Instead, at any f, separation out of a dense phase in a process that conserves f should be promoted by hydrophobic energy since the contacts between hydrophobic groups and water should decrease with increasing concentration of micelles and polyions. While favored also by electrostatic energy, it is counteracted by entropy especially when leading to a nonuniform distribution of small ions. However, the entropic penalty is removed in sufficiently concentrated systems and/or at sufficiently low f. By and large, this explains the shape and position of the biphasic region in Figure 3a.

Two features require further comments. One is the large difference in water content in coexisting phases in the biphasic region in the middle of the phase diagram. The difference is larger than expected for a transition driven mainly by aggregate repulsion and/or the packing constraints related to aggregate geometry. We attribute the effect to the hydrophobic attractions. This is supported by the observation that the NaPA−CTAPA−H_2O system, lacking strong hydrophobic attractions between micelles and polyion, displays a narrower two-phase region in the corresponding part of the phase diagram. The other feature is the small but distinct difference in f values between the coexisting phases in the biphasic region nearby the CTAPSS−H_2O axis. Clearly, in the presence of attractive forces, complexes are expected to phase separate when their charge density is sufficiently low. In principle, in the low f regime where this occurs, a transition conserving f could have been anticipated. The results from previous studies provide an explanation as to why this is not the case. The surfactant aggregation number in dilute dispersions has been found to decrease with increasing f, thereby increasing the area available for PSS to make contacts with the micelle. Thus, by adjusting the aggregation number, the hydrophobic energy in the dilute phase can remain low even when PSS is in excess ($f > 1$), at the same time allowing stoichiometric complexes ($f = 1$) to form a very dense phase with both low electrostatic and hydrophobic energy.

The intimate hydrophobic interaction between PSS and surfactants was demonstrated early by Kwak et al.[24] who showed that, in the dilute regime of the L_1 phase, the styrene group of the PSS backbone is incorporated in the micelle surface somewhere in the neighborhood of the first two methylene groups of surfactant's hydrocarbon tails. Later it was shown that this strongly reduced the surfactant aggregation number relative to that of free micelles.[20] This is in agreement with the results in Figure 11 showing that f affects the apparent radius of the cylinders in the H_1 phases, both in the P- and in the S-plane. This happens via its effect on the headgroup area per surfactant in the micelle, a_0. The binding of PSS to the micelle increases the distance between the head groups and thus increases a_0.

S-plane. In sharp contrast to the situation in the P-plane, where CTAPSS easily dissolves in the presence of NaPSS, the phase diagram in Figure 3b shows that the complex salt does not readily dissolve when CTAC is added. Instead, for a wide range of compositions it remains in a dense H_1 phase in equilibrium with an L_1 phase containing mainly CTAC and water. Interestingly, large amounts of CTAC can be incorporated in the complex phase without swelling the structure.

The results from earlier investigations strongly suggest that the stability and ordered phase structures of complex salts formed by hydrophilic polyions (mainly PA) and cationic surfactants in pure water result from a balance between attractive electrostatic and repulsive entropic forces. The attraction has been related to ion correlation and polyion bridging.[6,7,36] In a recent theoretical model of complex salts,[35] the repulsions were considered to have contributions from micelle−micelle excluded volume interactions and the entropy of mixing polyion and water. It was demonstrated that the translational entropy of the polyion played a major role

dx.doi.org/10.1021/jp212263b | J. Phys. Chem. B 2012, 116, 4634−4645

and thus that the density and the stability of the complex phase increased with increasing molecular weight of the polyion. Similar results were later found by dos Santos et al.[10] for a polyion−polyion complex salt (P^+P^-) using a modified Flory−Huggins theory. Importantly, their calculations also showed that the addition of a polyelectrolyte comprising monovalent counterions (P^+X^-) could dissolve the complex salt but only when the degree of polymerization of P^- was low. The influence of the degree of polymerization was found to be in qualitative agreement with that observed experimentally when surfactants (S^+X^-) are added to surfactant ion−polyion complex salts. Here, the surfactant micelles play the role of P^+. Clearly, the low electrostatic energy of water-poor complex salts and their small contribution to the entropy of mixing when made from high molecular weight polyions strongly limit their solubility. Thus, considering the high molecular weight of PSS used here, the large biphasic region in the S-plane in Figure 3b makes perfect sense. In general, one expects a high molecular weight complex salt to be difficult to dissolve unless at least one of the ions in the added electrolyte has a motive for associating with it. This is in agreement with early studies showing that large amounts of simple salt are needed to dissolve such complexes.[20,37] In the absence of specific interactions, the distribution of the added electrolyte should be governed chiefly by the entropy of mixing. The tie-lines in the biphasic region in Figure 3b indicate that the distribution of CTAC is largely determined by the chloride ion contribution to the entropy of mixing, except in the region close to the CTAPSS-H_2O axis (to be further discussed below). The tie-lines can be extrapolated to the CTAPSS corner of the phase triangle, showing that phase separation yields nearly the same CTAC/H_2O ratio in the phases. It means that the concentration of Cl^- is about the same in the aqueous subphases of both phases, and so no substantial swelling pressure builds up in the complex phase due to the partitioning of Cl^- between phases, explaining why CTAC is incorporated without swelling the structure. It also means that that CTAC is partitioned more to L_1 than to H_1, indicating that CTAC as a component has no strong affinity for the complex phase. A similar behavior is observed when C_nTAAc (n = 12, 16; Ac = acetate) is added to high molecular weight C_nTAPA−H_2O mixtures.[10] (Note, in the theoretical phase diagrams by dos Santos et al.,[10] the tie-lines are parallel to the complex salt−H_2O axis, a discrepancy possibly related to the implicit modeling of the micelles.)

Despite the similarities pointed out here, there are important differences between the PA and PSS systems, which can be ascribed to the hydrophobic backbone of the latter. In the biphasic region close to the binary CTAPSS−H_2O axis in Figure 3b, the tie-lines point to the H_2O corner of the phase diagram rather than to the CTAPSS corner, indicating that CTAC is preferentially partitioned to the dense phase. Clearly this must result in a higher Cl^- concentration in the aqueous subdomain in the dense phase than in the dilute phase and increased swelling pressure in the former. Remarkably, this is accompanied by a *lowering* of the water content of the dense phase. In contrast, when CTAAc is added to C_nTAPA, the tendency is to increase the water content, although the effect is very small when the molecular weight of PA is high. Interestingly, the effect observed here somewhat resembles that of adding CTAB to CTAPA, where the cubic phase in the binary CTAPA−H_2O system is transformed to a more dense H_1 phase, and where the tie-lines point to the H_2O corner in a large portion of the biphasic region.[5] Phase equilibrium requires that $c_{S^+}^{\text{dense}} c_X^{\text{dense}} = c_{S^+}^{\text{dilute}} c_X^{\text{dilute}}$, where c_i^{α} is the activity of ion i in phase α. Let the activities be represented by the concentrations of surfactant monomers and X^- in the aqueous subphases, respectively. Now, $C_{X^-}^{\text{dense}} > C_{X^-}^{\text{dilute}}$ implies $c_{S^+}^{\text{dense}} < c_{S^+}^{\text{dilute}}$. A lower monomer concentration in equilibrium with the micelles in the dense phase means a lower chemical potential of the surfactant ion and thus a driving force for incorporation of CTAX in the dense phase. Let us consider first the electrostatic driving force. The electrostatic energy of the surfactant ion should be lower in the dense than in the dilute phase, due to smaller average separation between the surfactant head groups and counterions. This should always favor partitioning of the surfactant ion to the dense phase, and may explain a tendency in this direction observed also when small amounts of C_{12}TAAc are incorporated in C_{12}TAPA complexes without swelling.[10] The quantitative results of the theoretical model mentioned above emphasize the importance of the *range* of repulsive and attractive forces in this respect.[35] In the pure complex salt of a high molecular weight polyion, the repulsion, within the model, is mainly provided by short-range micelle−micelle excluded volume interactions. These are balanced by electrostatic attractions of longer range, which means that, upon incorporation of excess of surfactant, the phase structure can tolerate a certain swelling pressure without absorbing water. However, it appears from the C_nTAAc/C_nTAPA systems that a substantial enrichment of surfactant in the dense phase, accompanied by depletion of water, requires more than the electrostatic driving force to compensate for the loss of entropy of the small ions. For CTAPA/CTAB, the extra driving force is probably related to the specificity of the bromide ion.[6,7,10] For CTAPSS/CTAC, the chloride ion is not likely to cause the effect, rather we ascribe it to the hydrophobic interaction between the polymer and the micelles. When PSS is in excess over the surfactant ($f > 1$; P-plane), Figure 11 shows there is a tendency to increase the area per surfactant to allow more of the polymer backbone to bind to the micelles. The tendency decreases with increasing amount of surfactant available, and when the surfactant is in sufficiently large excess (in the S-plane), the binding of PSS should not be limited by the area available. Instead there is free energy to be gained by packing the cylinders closer because it facilitates for the PSS chains to interact with more than one micelle. Indeed, Figure 11 also shows that the radius of the cylinder micelle increases with increasing hydrocarbon volume fraction but that the center−center distance between the micelles is almost unchanged, meaning that the distance between the surfaces of the cylinders decreases. Thus, a large fraction of the hydrophobic groups can remain intimately associated with the hydrocarbon core of the micelles and, at the same time, chains can form bridges between micelles without exposing a large fraction of hydrophobic groups to water. In this way, the system can accomplish both high chain entropy and low hydrophobic contact energy. An increased fraction of PSS segments bound to the micelles should also facilitate close packing of the micelles due to lower swelling pressure from the mixing of polymer chains and water.

The effects identified here, related to the hydrophobic interaction between polyion and micelles, should contribute to the observed deswelling of the CTAPSS complex phase. However, the enrichment of CTAC in the complex phase leading to a nonuniform distribution of Cl^- in the system should finally counteract the partitioning of CTAC to the complex phase. Indeed, when f decreases below 0.84, the slope of the tie-lines rapidly changes direction, and they tend instead to point to the CTAPSS corner (see Figure 3b). With the same reasoning as used above, the uniform distribution of Cl^- implies that the

dx.doi.org/10.1021/jp212263b | J. Phys. Chem. B 2012, 116, 4634−4645

chemical potential of the surfactant ion is the same in both phases in agreement with the conclusion above that in this region there is no preferential binding of CTAC to the complex phase. Instead, as already noted, the distribution of CTAC appears to be governed by the entropy of mixing of the chloride ions. Also in this range, the aggregate volume fraction increases with decreasing f (Figure 10), which should, at least to some extent, reflect the gradual removal of the swelling pressure from the Cl^- ions as their distribution becomes more uniform. However, the effects discussed above related to the hydrophobic (and electrostatic) interactions may continue to also contribute here.

The SAXS results suggest that there could be a narrow $H_1-H_1-L_1$ three-phase region close the CTAPSS–H_2O axis, and in that case there must be an additional H_1-H_1 two-phase region below it. The motive for a separation between two hexagonal phases with similar compositions is not obvious. In principle, the hydrophobic interactions discussed above could provide the driving force, but it cannot be precluded that samples are in a metastable state, in particular as the two H_1 phases could not be macroscopically separated from each other.

The samples in the $H_1-H_1-L_1$ three-phase region on the CTAC-rich side of the phase diagram separated macroscopically. The three-phase coexistence is a consequence of the L_1-H_1 disorder–order transition in the PSS-poor mixtures present already in binary CTAC–H_2O mixtures, and is thus believed to be caused mainly by excluded volume interactions and/or geometrical surfactant packing constraints. Thus we believe the H_1-H_1 phase separation has the same driving force as the phase separation in the large biphasic region discussed in detail above. The extension of this H_1-H_1 coexistence region toward the CTAC corner was not investigated. In principle, the composition of the phases may merge in a critical point. By considering the low water content in this part of the phase diagram, the region may also border on a lamellar phase-H_1 region.

CONCLUSIONS

We have studied phase behavior in mixtures of NaPSS, CTAC, and water, addressing the question of how the presence of the hydrophobic moiety (the benzene sulfonate group) on the polyion chain affects structures and phases in these mixtures. Only the disordered micellar and the ordered hexagonal phase were identified. Due to the highlighted specific feature of the polyion, the backbone of the PSS chain is embedded in the surface region of the micelles. We have ascertained that the interplay between electrostatic and hydrophobic interactions contributes to increased stability of the CTAPSS complex salt and leads to two partly competing strives of the system: to maximize the contact between PSS and the micelles and to form as dense phase as possible. The distinctive tendency to bind PSS^- to CTA^+ micelles promotes dissolution of CTAPSS when NaPSS is added (the P-plane) but to some extent stabilizes the dense phase when CTAC is added (the S-plane). Our work thus demonstrates that, despite the great tendency of oppositely charged polyion–surfactant ion systems toward associative phase separation, specific interaction between components can significantly alter this behavior.

ASSOCIATED CONTENT

Supporting Information

Phase diagram on the P-plane (Figure 3a) redrawn by plotting X_{Na^+} as a function of the total weight fraction of solid and the associated discussion. This material is available free of charge via the Internet at http://pubs.acs.org.

AUTHOR INFORMATION

Corresponding Author

*Address: Department of Chemistry and Biochemistry, Faculty of Chemistry and Chemical Technology, University of Ljubljana, Aškerčeva 5, P.O. Box 537 SI-1000 Ljubljana, Slovenia. Tel.: +(386-1)-2419-412. Fax: +(386-1)-2419-425. E-mail: ksenija.kogej@fkkt.uni-lj.si.

Notes

The authors declare no competing financial interest.

ACKNOWLEDGMENTS

This work was supported by the Slovenian Research Agency, ARRS, through the program Physical Chemistry P-0201. B.G. thanks FWO Vlaanderen for supporting the ESRF-DUBBLE, Big Science project. P.H. is thankful to the Swedish research council for financial support. The authors thank Prof. L. Piculell for valuable discussions and the Reviewers for additional ideas.

REFERENCES

(1) Lindman, B.; Thalberg, K. Polymer-Surfactant Interactions – Recent Developments. In *Interaction of Surfactants with Polymers and Proteins*; Goddard, E. D., Ananthapadmanabhan, K. P., Eds.; CRC Press: Boca Raton, FL, 1993; Chapter 5.

(2) Piculell, L.; Lindman, B.; Karlström, G. Phase Behavior of Polymer–Surfactant Systems. In *Polymer–Surfactant Systems*; Kwak, J. C. T., Ed.; Marcel Dekker, Inc.: New York, 1998; Chapter 3.

(3) Piculell, L.; Lindman, B. *Adv. Colloid Interface Sci.* **1992**, *41*, 149–178.

(4) Ilekti, P.; Martin, T.; Cabane, B.; Piculell, L. *J. Phys. Chem.* **1999**, *103*, 9831–9840.

(5) Svensson, A.; Piculell, L.; Cabane, B.; Ilekti, P. *J. Phys. Chem. B* **2002**, *106*, 1013–1018.

(6) Svensson, A.; Piculell, L.; Karlsson, L.; Cabane, B.; Jönsson, B. *J. Phys. Chem. B* **2003**, *107*, 8119–8130.

(7) Svensson, A.; Norrman, J.; Piculell, L. *J. Phys. Chem. B* **2006**, *110*, 10332–10340.

(8) Piculell, L.; Svensson, A.; Norrman, J.; Bernardes, J. S.; Karlsson, L.; Loh, W. *Pure Appl. Chem.* **2007**, *79*, 1419–1434.

(9) Norrman, J.; Lynch, I.; Picullel, L. *J. Phys. Chem. B* **2007**, *111*, 8402–8410.

(10) dos Santos, S.; Gustavsson, C.; Gudmundsson, C.; Linse, P.; Piculell, L. *Langmuir* **2011**, *27*, 592–603.

(11) Svensson, A.; Sjöström, J.; Scheel, T.; Piculell, L. *Colloids Surf. A: Phys. Eng. Aspects* **2003**, *228*, 91–106.

(12) Lynch, I.; Sjöström, J.; Piculell, L. *J. Phys. Chem. B* **2005**, *109*, 4258–4262.

(13) Andersson, M.; Råsmark, P. J.; Elvingson, C.; Hansson, P. *Langmuir* **2005**, *21*, 3773–3781.

(14) Kim, B.; Ishizawa, M.; Gong, J.; Osada, Y. *J. Polym. Sci. A: Polym. Chem.* **1999**, *37*, 635–644.

(15) Sasaki, S.; Yamazoe, Y.; Meada, H. *Langmuir* **2000**, *16*, 7126–7130.

(16) Magny, B.; Iliopoulos, I.; Zana, R.; Audebert, R. *Langmuir* **1994**, *10*, 3180–3187.

(17) Škerjanc, J.; Kogej, K. *J. Phys. Chem.* **1989**, *93*, 7913–7915.

(18) Škerjanc, J.; Kogej, K. In *Macroion Characterization. From Dilute Solutions to Complex Fluids*; Schmitz, K. S., Ed.; ACS Symposium Series 548; American Chemical Society: Washington, DC, 1994; Chapter 20, pp 268–275.

(19) Prelesnik, S.; Larin, S.; Aseyev, V.; Tenhu, H.; Kogej, K. *J. Phys. Chem. B* **2011**, *115*, 3793–3803.

(20) Hansson, P.; Almgren, M. *Langmuir* **1994**, *10*, 2115–2124.

(21) Kogej, K. *Adv. Colloid Interf. Sci.* **2010**, *158*, 68–83.

(22) Thalberg, K.; Lindman, B.; Karlstrom, G. *J. Phys. Chem.* **1991**, *95*, 6004–6011.

(23) Thalberg, K.; Lindman, B.; Bergfeldt, K. *Langmuir* **1991**, *7*, 2893−2898.
(24) Gao, Z.; Wasylishen, R. E.; Kwak, J. C. T. *J. Colloid Interface Sci.* **1988**, *126*, 371−376.
(25) Kogej, K.; Škerjanc, J. Surfactant Binding to Polyelectrolytes. In *Physical Chemistry of Polyelectrolytes*; Radeva, T., Ed.; Surfactant Science Series; Marcel Decker: New York, 2001; Vol. *99*, Chapter 21, pp 793−827.
(26) Škerjanc, J.; Kogej, K.; Vesnaver, G. *J. Phys. Chem.* **1988**, *92*, 6382−6385.
(27) Kogej, K.; Škerjanc, J. *Langmuir* **1999**, *15*, 4251−4258.
(28) Almgren, M.; Hansson, P.; Mukhtar, E.; van Stam, J. *Langmuir* **1992**, *8*, 2405−2412.
(29) Kogej, K.; Evmenenko, G.; Theunissen, E.; Škerjanc, J.; Berghmans, H.; Reynaers, H.; Bras, W. *Macrom. Rapid Commun.* **2000**, *21*, 1226−1233.
(30) Kogej, K.; Evmenenko, G.; Theunissen, E.; Berghmans, H.; Reynaers, H. *Langmuir* **2001**, *17*, 3175−3184.
(31) Huang, T. C.; Toraya, H.; Blanton, T. N.; Wu, Y. *J. Appl. Crystallogr.* **1993**, *26*, 180−184.
(32) Gommes, C. J.; Goderis, B. *J. Appl. Crystallogr.* **2010**, *43*, 352−355.
(33) Henriksson, U.; Blackmore, E. S.; Tiddy, G. J. T.; Söderman, O. *J. Phys. Chem.* **1992**, *96*, 3894−3902.
(34) Tanford, C. *The Hydrophobic Effect: Formation of Micelles and Biological Membranes*; Wiley: New York, 1973; p 52.
(35) Hansson, P. *J. Colloid Interface Sci.* **2009**, *332*, 183−193.
(36) Hansson, P. *Langmuir* **2001**, *17*, 4161−4167.
(37) Thalberg, K.; Lindman, B.; Karlstrom, G. *J. Phys. Chem.* **1991**, *95*, 3370−3376.